

## Heat capacity and transport measurements in sputtered niobium-zirconium multilayers

P. R. Broussard

*Naval Research Laboratory, Washington, D.C. 20375-5000*

D. Mael

*Bain and Co., 1 Embarcadero Plaza, San Francisco, California 94111*

(Received 9 March 1989)

We have studied the electrical resistivity and heat capacity for multilayers of niobium and zirconium prepared by magnetron sputtering for values of the bilayer period  $\Lambda$  varying from 4 to 950 Å. We find a transition in the thermal part of the resistivity that correlates with the coherent-to-incoherent transition seen in earlier work. The heat capacity data for the normal state show anomalous behavior for both the electronic coefficient  $\gamma$  and the Debye temperature. We also study the variation in  $T_c$  and the jump in the specific heat.

### INTRODUCTION

In an earlier paper<sup>1</sup> we looked at the specific heat for Nb-Zr multilayers for values of the bilayer period,  $\Lambda = d_{\text{Nb}} + d_{\text{Zr}}$ , where  $d_x$  is the thickness of layer  $X$ , in the range of 33–429 Å. In this paper we extend our measurements to samples with smaller values of  $\Lambda$ , including an essentially “alloy” sample ( $\Lambda = 4$  Å), and a sample with a larger value of  $\Lambda$ . In addition, we study the variation in the electrical resistivity, measured at room temperature and above the transition, and the superconducting critical temperature.

### SAMPLE PREPARATION AND STRUCTURE

The sample deposition technique has been described earlier<sup>1,2</sup> and will only be briefly described here. The multilayers are prepared by magnetron sputtering from separate Nb and Zr sources onto a substrate platform at ambient temperature which moves alternately between the two sources. During the deposition, we estimated the platform temperature would rise to approximately 100 °C. The deposition area was enclosed by a liquid-nitrogen cold shroud, which removed water vapor from the background environment, leaving  $\text{N}_2$ ,  $\text{CO}$ , and  $\text{CO}_2$  as the residual gases. The background pressure for the samples studied in the earlier work (Ref. 1) was  $\approx 1.5 \times 10^{-6}$  Torr, while for the new samples described here, the pressure was  $\approx 6 \times 10^{-7}$  Torr. The samples were sputtered in 2 mTorr of argon onto sapphire substrates. Deposition rates varied from 3–10 Å/s, and film thicknesses were between 1.1 and 1.6  $\mu\text{m}$ , depending on the value of  $\Lambda$ . Electron microprobe analysis indicated the samples had an atomic composition of 54.5 at. % Nb, which for bulk niobium and zirconium will give layers of nearly equal thickness.

The structure of these multilayers was studied thoroughly by Lowe and Geballe (Ref. 2). Our preliminary x-ray results agree with what was seen in their work. For  $\Lambda$  greater than 50 Å, the samples grow as (110) textured Nb layers and (002) textured Zr layers, stacked in-

coherently. As  $\Lambda$  decreases, the lattice undergoes a incoherent-to-coherent transition, with a single bcc lattice appearing. Lowe and Geballe estimated the amount of interdiffusion at the interface to be approximately 7 Å.

### ELECTRICAL RESISTIVITY MEASUREMENTS

The electrical resistivity of the samples was measured using the technique of Van der Pauw<sup>3</sup> at room temperature and at 10 K, where the resistivity was dominated by impurity scattering. The results of the measurements are shown in Fig. 1, where we plot the resistivity at 10 K, the residual resistivity ratio

$$RRR = \rho(T=300 \text{ K})/\rho(T=10 \text{ K})$$

and the thermal part of the resistivity,

$$\rho_{\text{th}} = \rho(T=300 \text{ K}) - \rho(T=10 \text{ K})$$

versus  $\Lambda$ . We see a clear saturation in the low-temperature resistivity and  $RRR$  as  $\Lambda$  decreases, indicating the interface contribution to the resistivity. We use Gurvitch's technique<sup>4</sup> for unfolding the individual resistivities in the layers for large  $\Lambda$  samples. We used our measured values from 1- $\mu\text{m}$ -thick films of Nb and Zr for the thermal part of the resistivity,  $\rho_x = 13.7$  and 41.6  $\mu\Omega \text{ cm}$  for Nb and Zr, respectively. The resistivity at 10 K for these films is 1.33  $\mu\Omega \text{ cm}$  for the Nb film and 25.2  $\mu\Omega \text{ cm}$  for the Zr film. For our initial analysis, we did not include the effect of resistivity saturation. The results of these calculations are shown in Fig. 2, where we plot the resistivity at 10 K for the layers versus the layer thickness. We will use the calculated values of the resistivity in our proximity-effect calculations. We found that the equations in Ref. 4 had no solution for our samples with  $\Lambda \leq 95$  Å. The results for the niobium layers, in Fig. 2(a), using a value of 370  $\mu\Omega \text{ cm Å}$  for the product of the resistivity and mean free path ( $\rho l$ ) in niobium,<sup>5</sup> indicate that the mean free path is less than the Nb layer thickness. The resistivity values for the zirconium layers show a turning over around  $d_{\text{Zr}} = 150$  Å, which seems unphysi-

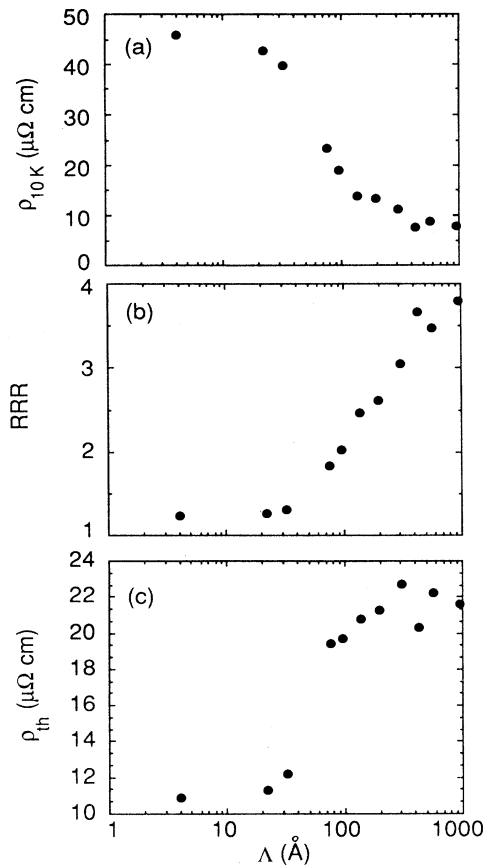


FIG. 1. (a) Electrical resistivity at 10 K vs  $\Lambda$ . (b) Residual resistivity ratio between room temperature and 10 K vs  $\Lambda$ . (c) Thermal part of the room-temperature resistivity vs  $\Lambda$ .

cal. Incorporating resistivity saturation or including a fixed interfacial alloy layer to the resistivity calculation does not change these results. We believe this is related to the behavior of the thermal part of the resistivity, described below. For the Zr layers, we do not have a good estimate for the  $\rho l$  product, but the free electron value is  $\approx 411 \mu\Omega \text{ cm } \text{\AA}$ , calculated from Eq. (10) in Ref. 4. Using this value, we find that the mean free path in the zirconium layers is substantially less than the Zr layer thickness.

The behavior of the thermal part of the resistivity in Fig. 1(c) is quite interesting. We see a sudden drop in  $\rho_{\text{th}}$  from a value of  $\approx 20 \mu\Omega \text{ cm}$ , which is about the average of the thermal parts for our niobium and zirconium films, to  $\approx 12 \mu\Omega \text{ cm}$ , which is close to that for the alloy sample, for  $\Lambda$  between 33 and 75  $\text{\AA}$ . A similar value for  $\rho_{\text{th}}$  was observed for a Nb-50 at. % Zr wire.<sup>6</sup> A simple explanation for this is that at some critical value of  $\Lambda$ , the interdiffusion is significant on the scale of the electrical resistivity. This would require for samples with  $\Lambda$  below this value (say  $\approx 50 \text{\AA}$ ) the interfacial layer dominates the period. If this is the case, then the critical temperatures of these samples, which average over longer-length scales than the electrical resistivity, would be the same as

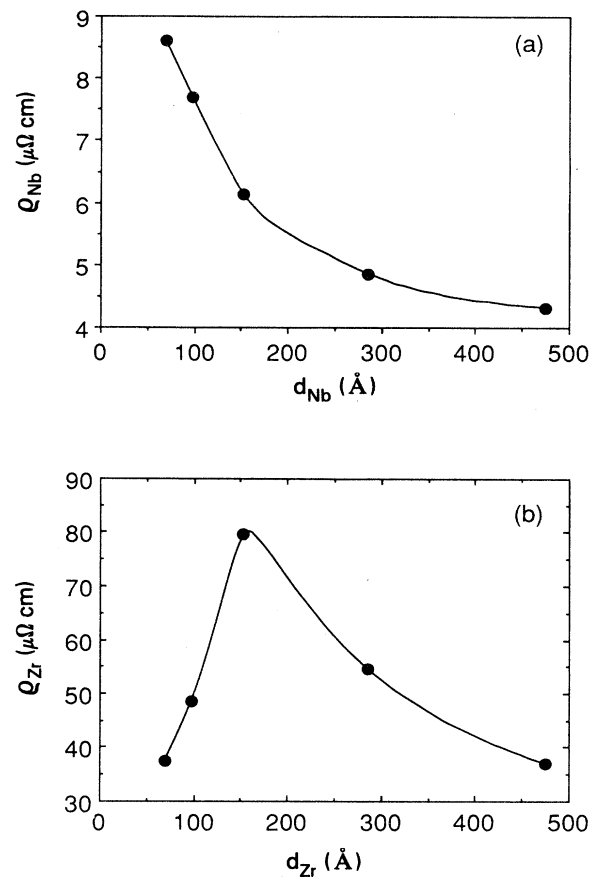


FIG. 2. Calculated values for the in-plane resistivities at 10 K vs the layer thickness for (a) the niobium layers and (b) the zirconium layers. The lines are guides to the eye.

the alloy sample. We will see that this is not the case. We will come back to this point when we discuss the normal-state parameters in the specific heat.

#### SPECIFIC HEAT MEASUREMENTS

The measurement details for the specific heat have been presented elsewhere<sup>1,7</sup> and will not be presented here. Data were taken for the samples with  $\Lambda = 4, 22, 32.8, 95, 195, 429, \text{ and } 950 \text{\AA}$ . These data are shown in Figs. 3 and 4, plotted as  $C/T$  versus  $T^2$ . The analysis for the normal-state properties and superconducting parameters is as previously described.<sup>1</sup> The figures also show the resulting fits to the normal state. We point out that the normal-state parameters are determined above  $T_c$ .

Figure 5 shows the values obtained for the electronic coefficient of specific heat,  $\gamma$ , and the Debye temperature,  $\Theta_D$ . From our bulk Nb and Zr films, we have  $\gamma = 7.8$  and  $2.8 \text{ mJ/mole K}^2$  and  $\Theta_D = 265$  and  $275 \text{ K}$  for niobium and zirconium, respectively. Notice that we have not accounted for the change in slope of  $C/T$  versus  $T^2$  observed in niobium near 3 K (Ref. 8). For large values of  $\Lambda$ , both  $\gamma$  and  $\Theta_D$  tend toward the molar average of niobium and zirconium,  $5.6 \text{ mJ/mole K}^2$  and  $269 \text{ K}$ , re-

spectively. We notice, as in Ref. 1, that the value for  $\Theta_D$  is still quite depressed from the molar average even for  $\Lambda=950 \text{ \AA}$ . We still do not have a good explanation for this behavior. As  $\Lambda$  decreases, the values of  $\gamma$  and  $\Theta_D$  do not go smoothly from their averages to the values for the "alloy" sample,  $\gamma=6.75 \text{ mJ/mole K}^2$  and  $\Theta_D=210 \text{ K}$ . In fact there is a peak in  $\gamma$  and a dip in  $\Theta_D$  at approximately the same value of  $\Lambda \approx 20\text{--}30 \text{ \AA}$ . This is also the same point where we saw the drop in the thermal part of the resistivity in Fig. 1 and where the coherent-to-incoherent transition was seen in Ref. 2. In Ref. 2, at this point the Zr hcp phase had disappeared completely, and was replaced by a single bcc phase in the sample. This transition may result in the anomalies observed here. We point out that other systems have exhibited structural changes, for example Nb/Cu<sup>9</sup>, Mo/Ni<sup>10</sup>, and Mo/Ta<sup>11</sup>, in approximately the same thickness range, showing a lattice softening in Brillouin scattering experiments.

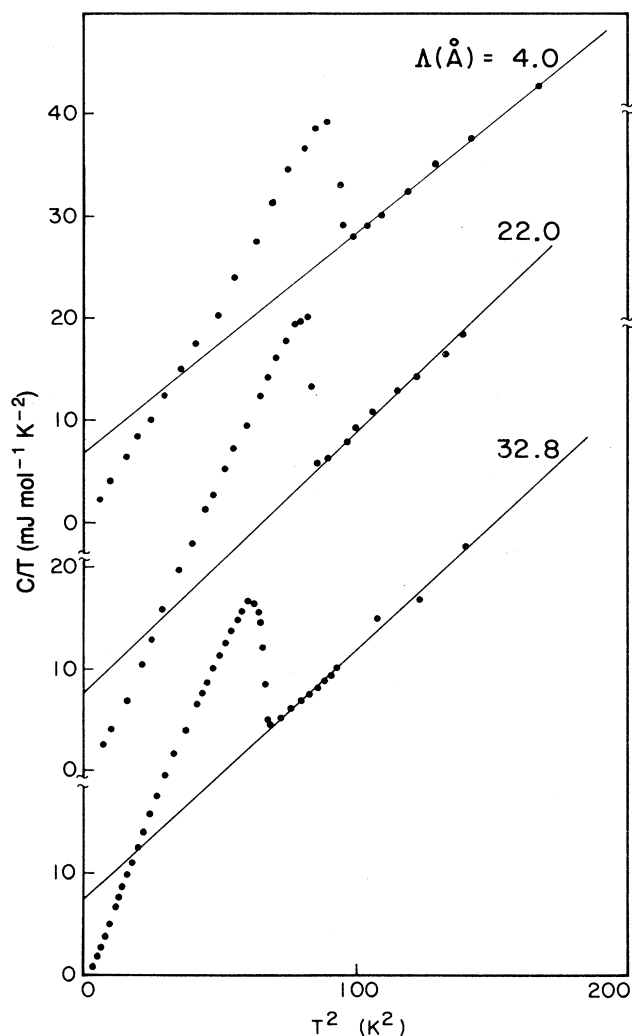


FIG. 3. Specific heat plotted as  $C/T$  vs  $T^2$  for the small  $\Lambda$  samples. The lines are the fits to the normal-state data, and the curves are offset for clarity.

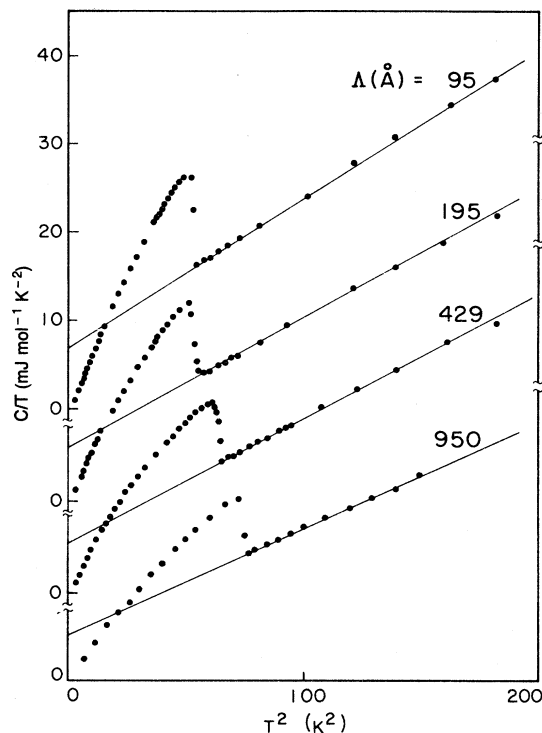


FIG. 4. Same as Fig. 3 for the large  $\Lambda$  samples.

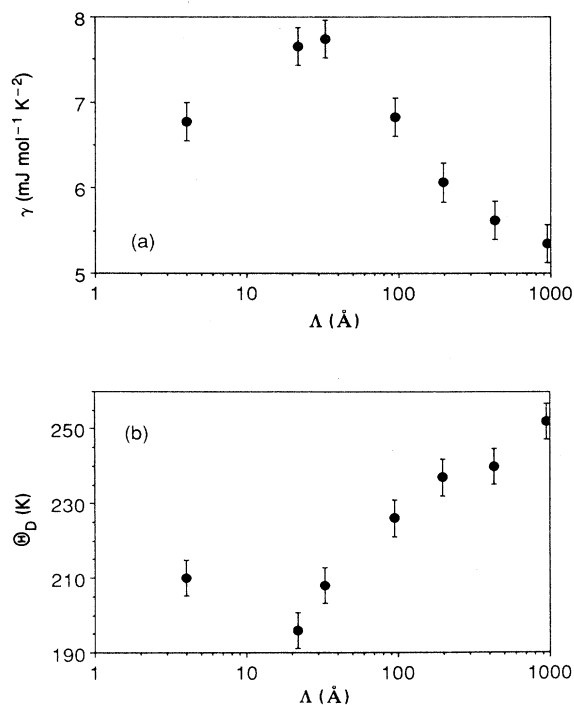


FIG. 5. Normal-state parameters determined above  $T_c$  vs  $\Lambda$ . (a) the electronic coefficient of the specific heat, and (b) the Debye temperature.

Figure 6 shows the superconducting parameters found from the specific-heat data, namely, the superconducting transition temperature,  $T_c$ , and the value of the jump at the transition,  $\Delta C/\gamma T_c$ . In Fig. 6(a) we also include  $T_c$ 's measured resistively for those samples whose specific heat was not measured. For small  $\Lambda$  we see the effect of the interfacial NbZr alloy, causing a rise in  $T_c$  up to 9.7 K. Clearly however, the  $T_c$  drops as  $\Lambda$  increases, down to  $\approx 7.2$  K for  $\Lambda = 200$  Å. As mentioned earlier, if the drop in the thermal part of the resistivity was due to extreme interdiffusion between the layers, then the  $T_c$  at those values of  $\Lambda$  would also reflect that degree of interdiffusion. Clearly the observed  $T_c$ 's show that interdiffusion is not sufficient to explain the sudden drop in  $\rho_{th}$ . As  $\Lambda$  increases, we see an increase in  $T_c$  due to the proximity effect.

We can model the variation in the  $T_c$  with respect to  $\Lambda$  by using the standard de Gennes–Werthamer proximity effect analysis, as was presented in earlier work on Nb/Ta.<sup>12</sup> Here we use the dirty limit approximation since the mean free path in both layers is smaller than the coherence lengths. As in Ref. 12 we do not incorporate the infinite multilayer modification, where one replaces the layer thicknesses by  $\frac{1}{2}$  their value but use the standard bilayer model. This is consistent with the calculations done by Menon and Arnold<sup>13</sup> where the  $T_c$  for a superlattice was found to be the same as or slightly higher

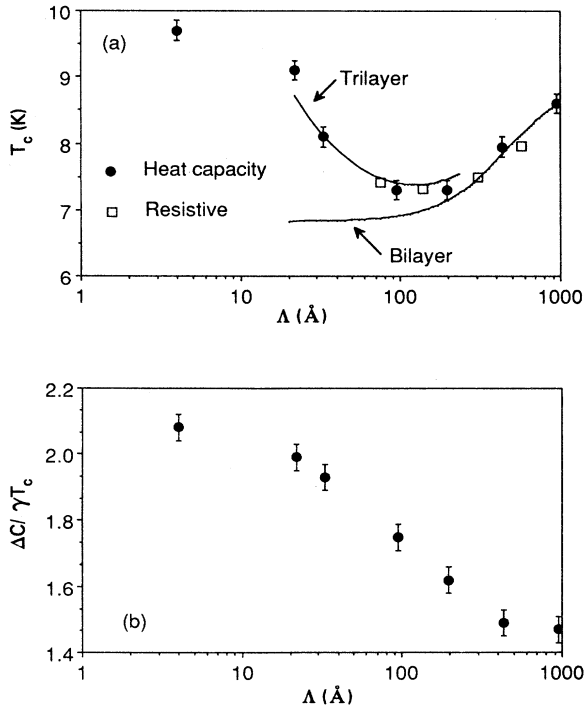


FIG. 6. Superconducting parameters for the samples vs.  $\Lambda$ . (a) The superconducting transition temperature, determined either by specific heat or resistivity measurement, and (b) the normalized jump in the specific heat. The curves are described in the text.

than a bilayer with the same layer thicknesses. For our case, we stay with the bilayer model, which gives for our equation set

$$\begin{aligned}\chi(\xi_S^2 q_S^2) &= \ln(T_{cS}/T_c), \\ \chi(-\xi_N^2 q_N^2) &= \ln(T_{cN}/T_c), \\ q_S \tan q_S d_S &= \eta q_N \tanh q_N d_N, \\ \xi_{S,N} &= \left[ \frac{\hbar(v_F l)_{S,N}}{6\pi k_B T_c} \right]^{1/2} \\ &= \frac{54493}{(\rho\gamma T_c)^{1/2}} \quad (\text{in } \text{Å}),\end{aligned}$$

where the last equation is derived from the equations listed by Orlando *et al.*,<sup>14</sup>  $\rho$  is given in  $\mu\Omega$  cm, and  $\gamma$  is given in  $\text{ergs}/\text{cm}^3 \text{K}^2$ . As in Ref. 11, the value of  $\eta$  is given by

$$\begin{aligned}(\gamma\xi^2)_{\text{normal}}/(\gamma\xi^2)_{\text{superconducting}}, \\ \chi(z) = \Psi(\frac{1}{2} + z/2) - \Psi(\frac{1}{2}),\end{aligned}$$

and

$$d_S + d_N = \Lambda.$$

The curve labeled bilayer in Fig. 6(a) is calculated using the preceding equations and our measured values for  $\gamma$  and  $\rho$  for pure Nb and Zr films. We see that this curve seems to agree quite well for those samples with  $\Lambda > 200$  Å. We can also do the calculation using the inferred values of layer resistivities as shown in Fig. 2 for samples with  $\Lambda \geq 138$  Å, using both the bilayer calculation and the infinite multilayer calculation. These results are shown in Table I. We must point out that the values for  $\Lambda = 138$  and 195 Å use values of  $\rho_{Zr}$  which seem anomalous, as pointed out before. We can see from Table I, that while the agreement with the measured values is not excellent for either column, the bilayer column agrees slightly better with the experimental results.

For the  $T_c$  measurements below  $\Lambda = 200$  Å, we use the approach given in the work by Triscone *et al.*<sup>15</sup> for a trilayer system. The curve labeled trilayer in Fig. 6(a) is calculated using a 7-Å interfacial alloy having the same parameters as measured for our alloy sample. We see that the curve agrees reasonably well with the data, especially in predicting where the turnover in the transition temperature occurs. This value of interfacial width is the same as that determined in Ref. 2.

TABLE I. Comparison of calculated transition temperatures.

$\Lambda$ (Å)	Measured $T_c$ (K)	Calculated $T_c$ (K)	
		Bilayer	Infinite multilayer
950	8.60	8.69	8.12
570	7.95	8.45	7.77
429	7.95	8.28	7.56
305	7.50	8.03	7.34
195	7.30	7.37	6.99
138	7.32	7.08	6.89

The specific-heat jump,  $\Delta C/\gamma T_c$  in Fig. 6(b), shows a decrease as  $\Lambda$  increases, tending toward the value one would expect if there were no proximity effect (NPE) present, which for our films would give a value of 1.51. The theories for the specific heat of a bilayer system,<sup>16,17</sup> predict that  $\Delta C/\gamma T_c$  will decrease from the NPE limit as  $\Lambda$  decreases, while we see the opposite. This calculation did not include a variation in the density of states or  $T_c$  with  $\Lambda$ , but the variation we see would not account for the disagreement. The question then arises as to whether, even in the large  $\Lambda$  limit, the system is in the NPE limit, i.e., is it simply a coincidence that at large  $\Lambda$  the value of  $\Delta C/\gamma T_c$  is close to the NPE value. We can observe this by examining the superconducting electronic part of the specific heat,  $C_{es}$ , which is determined by subtracting out the lattice contribution, and finally subtracting out the extrapolated residual normal electronic specific heat. Figure 7 shows the residual normal electronic specific heat as a function of  $\Lambda$ . Clearly, at small values of  $\Lambda$ , the entire sample is superconducting, but as  $\Lambda$  increases, we find evidence of normal electronic specific heat indicating the presence of normal Zr in our films. This is consistent with the idea that large enough  $\Lambda$ , the value of the order parameter has become low enough in the middle of the Zr layers to show a contribution to the normal electronic specific heat. However, it is important to note that not all of the Zr is normal yet, or else the residual  $\gamma$  would reach 1.22 mJ/mole K<sup>2</sup>, the value expected for a system of equal thickness superconducting Nb and normal bulk Zr layers.

With this analysis complete, we can look at the superconducting part of the electronic specific heat,  $C_{es}(T)$ , shown in Fig. 8, which shows the results from the two extremes of the layered system (22 and 950 Å), the result for our Nb film, which serves as a model for the shape of a strongly coupled  $C_{es}(T)$  curve, and the BCS curve for  $C_{es}(T)$ , which will model the shape for weak coupling. Figure 9 shows fits to the obtained  $C_{es}(T)$  for some of the

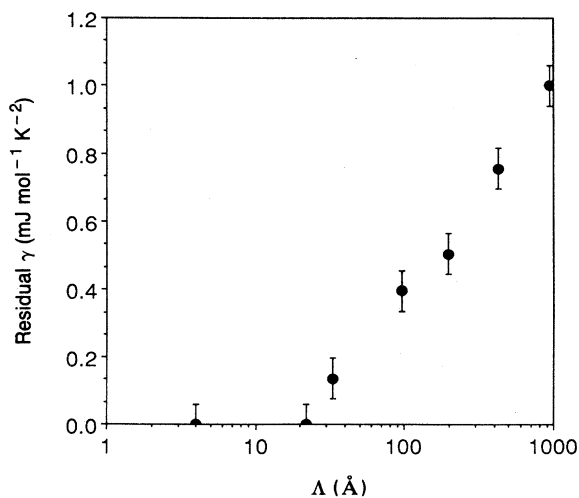


FIG. 7. The residual normal-state electronic specific-heat coefficient vs  $\Lambda$ .

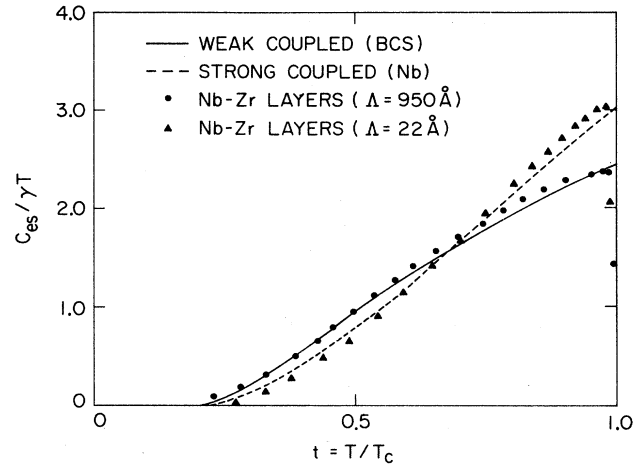


FIG. 8. The superconducting electronic specific heat for  $\Lambda=22$  and 950 Å, compared with the value for a bulk Nb film (strongly coupled) and the BCS prediction.

other samples.

From Refs. 16 and 17, we would expect in the large  $\Lambda$  limit the system would tend towards the NPE limit, which for our case should be layers of strongly coupled fully superconducting Nb and normal Zr. In this case,  $C_{es}$  would resemble that for Nb, but reduced by the resulting molar fraction of Nb. As  $\Lambda$  decreases, the proximity effect with the Zr layers should make the system behave like a weakly coupled superconductor, with a correspondingly reduced value for  $\Delta C/\gamma T_c$ , and so should it begin to resemble the BCS curve. We clearly see from Figs. 8 and 9 that this is not the case. At small values of  $\Lambda$ , the shape of  $C_{es}(T)$  resembles that of a strongly coupled superconductor (pure Nb), while for the largest  $\Lambda$ , the curve resembles the BCS result almost exactly. Figure 9 shows this trend from strong to weak coupled as  $\Lambda$

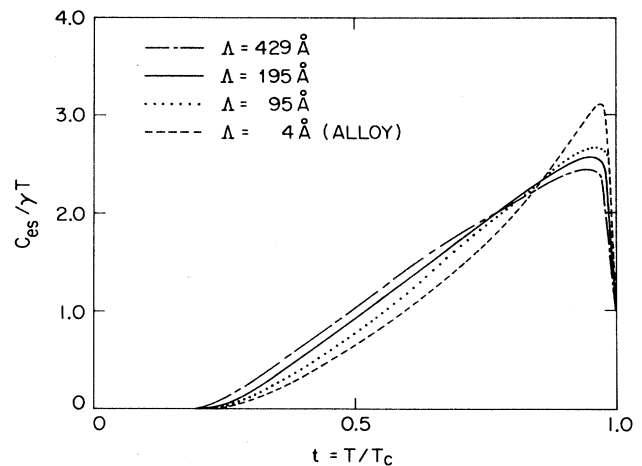


FIG. 9. Fits to the superconducting electronic specific heat for the other values of  $\Lambda$ .

increases. Obviously, at small  $\Lambda$ , the presence of a strongly coupled NbZr alloy leads to the large values of  $\Delta C/\gamma T_c$  and the corresponding shape of  $C_{es}$ . For our large  $\Lambda$  sample, we have seen from our proximity-effect calculations that the decay length into the Nb is  $\approx 500 \text{ \AA}$ , indicating that the proximity effect is still quite strong in this sample, which may cause the system still to act as a weakly coupled system. What is surprising is that if the theory for  $C_{es}$  is correct, then in the range of large  $\Lambda$ , where the interface contribution is small, we should see the expected decrease in the specific heat jump as  $\Lambda$  decrease, which we clearly do not.

### CONCLUSIONS

Our measurements of the electrical resistivity in these samples show that the electron mean free path at low temperatures is smaller than the layer thicknesses. There is an anomalous transition in the thermal part of the electrical resistivity between 33 and 75  $\text{\AA}$ , which is in the same range where the incoherent-to-coherent transition was seen earlier. The superconducting critical temperatures are well described by the proximity-effect model as-

suming a bilayer equation for  $\Lambda > 138 \text{ \AA}$ , and a trilayer model with a 7- $\text{\AA}$  interfacial layer for  $\Lambda < 138 \text{ \AA}$ .

The normal-state specific heat, in the limit of large  $\Lambda$ , tends towards the bulk average for Nb and Zr, but as  $\Lambda$  decreases, we see anomalies in both the Debye temperature and the electronic specific heat coefficient, at approximately the same value of  $\Lambda$  where the anomaly in  $\rho_{th}$  occurred. As with the transition in the thermal part of the resistivity, we believe these are due to the lattice transition seen by Lowe and Geballe. The superconducting part of the specific heat shows a transition from weakly coupled to strongly coupled as  $\Lambda$  decreases, which is the opposite of that expected from the current theories.

### ACKNOWLEDGMENTS

We would like to thank Ted Geballe for many helpful discussions and crucial support. This work was supported principally by the Air Force Office of Scientific Research. Samples were prepared at the Stanford University Center for Materials Research, under the support of the National Science Foundation Materials Research Laboratories Program.

<sup>1</sup>P. R. Broussard, D. Mael, and T. H. Geballe, *Phys. Rev. B* **30**, 4055 (1984).

<sup>2</sup>W. P. Lowe and T. H. Geballe, *Phys. Rev. B* **29**, 4961 (1984).

<sup>3</sup>L. J. Van der Pauw, *Philips Res. Rep.* **13**, 1 (1958).

<sup>4</sup>M. Gurvitch, *Phys. Rev. B* **34**, 540 (1986).

<sup>5</sup>P. R. Broussard and T. H. Geballe, *Phys. Rev. B* **35**, 1664 (1987).

<sup>6</sup>D. J. Evans and R. A. Erickson, *J. Appl. Phys.* **36**, 3517 (1965).

<sup>7</sup>D. Mael, Ph.D. dissertation, Stanford University, 1987 (unpublished).

<sup>8</sup>R. L. Cappelletti, N. Wakabayashi, W. A. Kamitakahara, J. G. Traylor, and A. J. Bevolo, *Phys. Rev. B* **25**, 6096 (1982).

<sup>9</sup>A. Kueny, M. Grimsditch, K. Miyano, I. Banerjee, C. M. Falco, and I. K. Schuller, *Phys. Rev. Lett.* **48**, 166 (1982).

<sup>10</sup>M. R. Khan, C. S. L. Chun, G. P. Felcher, M. Grimsditch, A. Kueny, C. M. Falco, and I. K. Schuller, *Phys. Rev. B* **27**, 7186 (1983).

<sup>11</sup>J. A. Bell, W. R. Bennett, R. Zanoni, G. I. Stegeman, C. M. Falco, and F. Nizzoli, *Phys. Rev. B* **35**, 4127 (1987).

<sup>12</sup>P. R. Broussard and T. H. Geballe, *Phys. Rev. B* **37**, 60 (1988).

<sup>13</sup>M. Menon and G. B. Arnold, *Superlattices and Microstructures* **1**, 451 (1985).

<sup>14</sup>T. P. Orlando, E. J. McNiff, Jr., S. Foner, and M. R. Beasley, *Phys. Rev. B* **19**, 4545 (1979).

<sup>15</sup>J.-M. Triscone, D. Ariosa, M. G. Karkut, and Ø. Fisher, *Phys. Rev. B* **35**, 3238 (1987).

<sup>16</sup>M. P. Zaitlin, *Solid State Commun.* **41**, 317 (1982).

<sup>17</sup>M. P. Zaitlin, *Phys. Rev. B* **25**, 5729 (1982).